Coupled Systems Mechanics, *Vol. 3, No. 1 (2014) 73-88*
DOI: http://dx.doi.org/10.12989/csm.2014.3.1.073

Modelling and numerical simulation of concrete structures subject to high temperatures

Lars Ostermann* and Dieter Dinkler**

Institut für Statik, Beethovenstrasse 51, 38106 Braunschweig, Germany

(Received November 11, 2013, Revised January 25, 2014, Accepted March 10, 2014)

Abstract. The paper deals with a model founded on the physical processes in concrete subject to high temperatures. The model is developed in the framework of continuum damage mechanics and the theory of porous media and is demonstrated on selected structures. The model comprises balance equations for heat transfer, mass transfer of water and vapour, for linear momentum and for reaction. The balance equations are completed by constitutive equations considering the special behaviour of concrete at high temperatures. Furthermore, the limitation and decline of admissible stresses is achieved by using a composed, temperature depending crack surface with a formulation for the damage evolution. Finally, the complete coupled model is applied to several structures and to different concrete in order to determine their influence on the high-temperature-behaviour.

Keywords: concrete; high temperatures; coupled thermo-mechanical-chemical damage

1. Introduction

In the last decades severe fires occur in highly frequented buildings and leads to a large number of casualties and damage of infrastructure. Here, the destruction of the First Interstate Bank building (Los Angeles 1998), the World Trade Center (New York 2001), the Ostankino Tower (Moscow 2000, 2007) and of many others show the high risk and the high damage potential of buildings without sufficient damage protection against catastrophic fire accidents.

The increasing number of severe fires in multi-storey buildings and tunnel structures, which mainly consist of concrete in the load bearing structural members, shows the need for an a priori analysis of the concrete structures. Especially, in multi-storey buildings the evacuation and the firefighting are in many cases difficult due to narrow escape routes. During the firefighting the load bearing capacity of the fire exposed structures and of the whole building are of utmost importance at any time during and after the fire in the affected building.

Heat inflow during fires leads to high temperatures in those sections of concrete structures, which are close to the fire-exposed surface. Concrete is a porous material and contains adsorbed water in its pores. Due to high temperatures, the adsorbed water evaporates rapidly, so the pore pressure increases immediately. Besides, high temperatures cause a dehydration of the cement

*Corresponding author, Ph. D., E-mail: statik@tu-braunschweig.de
** Professor, E-mail: statik@tu-braunschweig.de

http://www.techno-press.org/?journal=csm&subpage=7 ISSN: 2234-2184 (Print), 2234-2192 (Online)

paste along with an additional vapour release and lead to a further increase of the pore pressure. The high values of pore pressure and the dehydration of cement paste severely damage the concrete structure and entail spalling of the fire-exposed surface.

Several approaches of different complexity exist for the modelling of concrete subject to high temperatures. The following theoretical approaches emphasise that the description of the complex phenomenology of concrete subject to high temperatures is possible with reasonable assumptions.

A simplified approach to model heat and mass transport show Bazant *et al*. (1981). The authors use a diffusion-convection-equation for the description of moisture transport without a detailed description of transport of vapour, which is necessary to predict the spalling of concrete due to excess vapour pressure.

A very detailed model for concrete subject to high temperatures is presented by Gawin *et al*. (2003). This model bases on the balance equations for the mass of water, vapour, dry air, for the energy and the momentum, see also Lewis and Schrefler (1998). The combined balance equation of pore water and vapour contains the vapour release due to dehydration and the evaporation of pore water. The evolution of porosity, which increases in a consequence of dehydration, is formulated by Gawin *et al*. (2003) with a change in the density of the solid phase of concrete. The balance of energy comprises diffusive and convective flows, latent heat and heat of reaction due to dehydration. In this model the capillary pressure, the gas pressure and the temperature as independent variables describe the phase transition for the whole temperature range, even beyond the critical temperature of water. For the evolution of mechanical damage, Gawin *et al*. (2003) chose an isotropic explicit non-local integral formulation, which result along with the temperature-dependent thermo-chemical damage in the total damage. The pore pressure is coupled with the Cauchy stress by means of the Biot-number.

Furthermore, the evolution of strain components resulting from different physical phenomena influence the mechanical behaviour of the heat exposed concrete is explained by Khoury (2006). Khoury (2006) distinguishes for unloaded concrete between smeared crack, thermal strains, drying shrinkage and dehydration shrinkage. At loaded state, additionally, elastic and load induced thermal strains occur as well as creep strains and plastic strains. Hence, the strain model of Khoury (2006) allows a detailed characterisation of strains and especially irreversible strains in concrete at high temperatures.

2. Model for the macroscopic behaviour of concrete at high temperatures

In this paper a mathematical-physical, fully coupled model is presented, which is able to predict the behaviour of concrete structures at fire impacts by means of numerical simulation and analysis of the transport and reaction processes and the deformation behaviour, see Fig. 1. This requires the basic balance equations for energy, momentum, and mass with special consideration of pore water and vapour. The mechanical model for concrete at high temperatures considers the increasing pore pressure, the thermally induced strains and the mechanical degradation due to the dehydration and the critical mechanical loads. Furthermore, all models need an accurate description and verification of the material parameters considering the influence of the composition of concrete and state variables as temperature. The thermal dehydration of cement paste affects the transport processes and the mechanical behaviour.

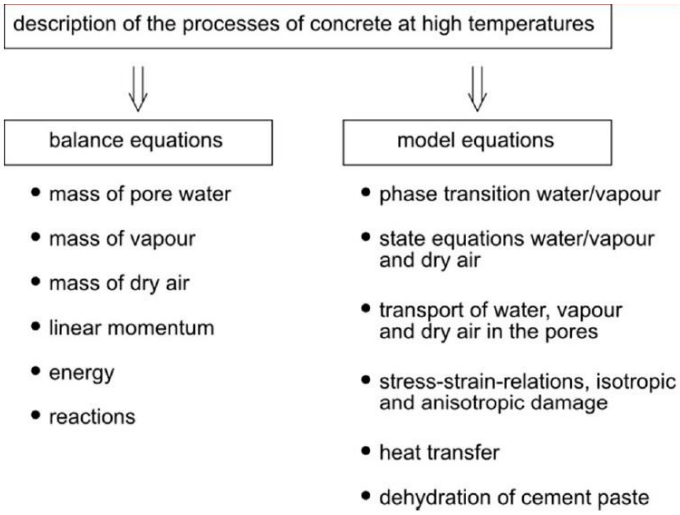

Fig. 1 Model equations for concrete subject to high temperatures

The balance equations result from the theory of porous media and are formulated for the mass of pore water, the mass of pore gas, and for the energy, see Lewis and Schrefler (1998) and Ostermann (2012). The constitutive equations for storage and transport are formulated by means of phenomenological approaches and afterwards inserted into the balance equations. In the model for advective mass transport of pore water and pore gas, Darcy's law is applied, see Gawin *et al*. (2003). For the description of diffusion of pore gas within the pores, the flow model of Fick is adopted and, similarly, Fourier's law is applied to model the diffusive energy transport.

The mechanical behaviour of concrete is very complex because of its internal heterogeneous structure of porous cement paste and mineral aggregates. Hence a phenomenological approach is chosen for the model, which founded on the theory of plasticity and of continuum damage mechanics. For limiting the admissible stresses, a combined yield surface of Rankine and Drucker-Prager criteria is used to reproduce the brittle failure due to tensile stress and the ductile behaviour due to compressive stresses. Beside the elastic and irreversible strains, thermal and hygric strains are included in the mechanical model (Gawin *et al*. 2003). For the numerical analysis the model for the mechanical behaviour is implemented by means of a non-local approach for the irreversible strains, so that a unique solution at mechanically degrading material is achieved (Peerlings *et al*. 1998).

The dehydration of the cement paste due to high temperatures is directly related to the temperature, since rate effects of the dehydration can be neglected. The degree of dehydration can be formulated as a function of temperature and cement composition as the temperature increases. The vapour release resulting from the dehydration reaction is considered in the mass balance of water and vapour. Furthermore, the chemical damage describes the mechanical degradation of the cement paste as a result of the dehydration.

3. Model equations

The theoretical model is dealing with the governing equations for balance of mass, momentum and energy in order to describe the phenomenology of transport, reaction and mechanical behaviour.

The flow of vapour is driven by the gradient of pressure and of concentration. The flow of pore water is phenomenologically described by the law of Darcy. Especially, as a consequence of dehydration the pores in the cement paste enlarge, hence the flow due to the pressure gradients dominates the molecular flow at very narrow pores. Nonetheless, the flow at very narrow pores is described by the same approach but with different material parameters.

3.1 Transport equations

The essential phenomena in the behaviour of concrete at high temperature are described by balance equations. The mass balance enables the description of transport of water and gas within the pores of concrete. In order to cover the transport of water, vapour and dry air the corresponding mass balance equations are necessary. The equations for water and vapour can be condensed, the source term from phase transition vanishes, see Gawin *et al*. (2003).

$$\begin{aligned} & n\frac{\mathrm{D}^s}{\mathrm{D}t}\left(S_w\,\rho_w + S_g\,\rho_v\right) + \nabla\cdot\left(\mathbf{q}_w + \mathbf{q}_v + \mathbf{q}_{va}\right) + \left(S_w\,\rho_w + S_g\,\rho_v\right)\nabla\cdot\mathbf{v}_s \\ & = c_v + \left(S_w\,\rho_w + S_g\,\rho_v\right)\left(\frac{c_{s,deh}}{\rho_s} + \frac{1-n}{\rho_s}\frac{\mathrm{D}^s\rho_s}{\mathrm{D}t}\right) \end{aligned} \tag{1}$$

Here n is the porosity, S_w the saturation of water, S_g the saturation of gas, ρ_w the density of water, ρ_v the density of water, ρ_s the density of the solid phase, $\mathbf{q}_w$ the flow of water, $\mathbf{q}_v$ the flow of vapour, $\mathbf{q}_{va}$ the diffusive flow of dry air, $\mathbf{v}_s$ the velocity of the solid phase, c_v the vapour release from dehydration, and $c_{s,deh}$ the change of solid mass due to dehydration.

The heat transfer within the structure is described with the conservation equation of energy

$$C_{p,\underset{concr}{beton}}\frac{\partial T}{\partial t} + \left(c_{pw}\,\mathbf{q}_w + c_{pg}\left(\mathbf{q}_a + \mathbf{q}_v\right)\right)\cdot\nabla T - \nabla\cdot\mathbf{q}^e + J_w^m\,\Delta h_{vap} + c^e_{s,deh} = 0 \tag{2}$$

Here $C_{p,concr}$ is the heat capacity of concrete, c_{pw} the heat capacity of water, c_{pg} the heat capacity of gas, T the temperature, $\mathbf{q}^e$ the diffusive heat flow, $J^m{}_w$ the rate of mass change of water, Δh_{vap} the latent heat, and $c^e{}_{s,deh}$ the heat of dehydration.

The balance equations can be written in terms of the independent variables if constitutive equations for primary and secondary variables are applied, see Gawin *et al*. 2003.

3.2 Modelling transport phenomena and reaction processes

The model for the transport requires several types of constitutive equations. First, formulations concerning the storage terms in the balance equations describe the change of density, pore water saturation and enthalpy. The formulation for the density of pore water follows the constitutive equations stated by IAPWS (1994). The saturation depends on the initial pore structure. The dehydration does not influence the saturation since the temperature ranges, where pore water occurs and dehydration takes place, do not coincide.

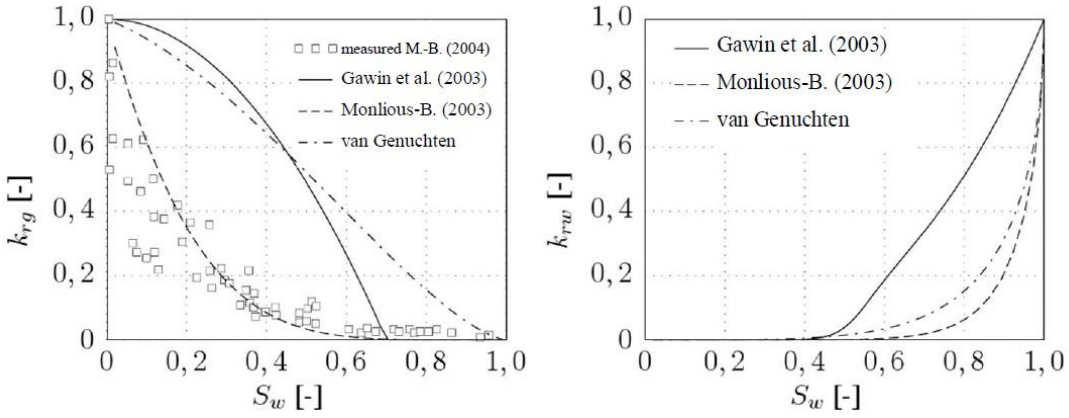

Fig. 2 Relative permeability for gas and liquid phase k_{rg} and k_{rw} in concrete

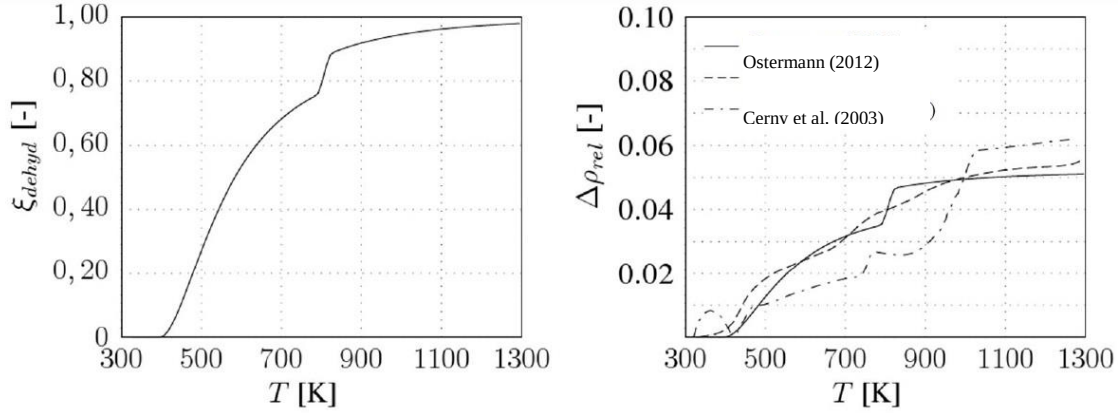

Fig. 3 Degree of dehydration ξ_{dehyd} and change in density ρ_{rel}

The relative permeability is one of the key parameters in the transport model, see Fig. 2. The relative permeability k_{rg} for the gas phase decreases with increasing saturation of water in the pores. In contrast the relative permeability of water increases at the upper range of water content.

The degree of dehydration of cement minerals is composed of two separate dehydration processes. Because of the amorphous structure of the CSH phase its dehydration occurs gradually over a wide range of temperature. In the model, the dehydration of all other cement mineral components except Portland it is correlated to the dehydration CSH phase with the parameters $T_{0,CSH}$ = 470 K and a_{CSH} = 2,5.

$$\xi_{CSH}(T) = \begin{cases} 0\,, & T < T_{0,CSH}\,, \\ \frac{1}{2}\left(1 - \cos\left(\pi - \pi\left(\frac{T_{0,CSH}}{T}\right)^{a_{CSH}}\right)\right), & T \geq T_{0,CSH}\,, \end{cases} \tag{3}$$

In contrast to the CSH phase the dehydration of the portlandit, which represent also an important component of the cement minerals, takes place in a narrow temperature range. The

model parameters for portlandit are $T_{0,CH}$ = 760 K, $T_{1,CH}$ = 800 K.

$$\xi_{CH}(T) = \begin{cases} 0\,, & T < T_{0,CH}\,, \\ \frac{1}{2}\left(1 - \cos\left(\frac{T - T_{0,CH}}{T_{1,CH} - T_{0,CH}}\right)\right), & T_{0,CH} \le T \le T_{1,CH}\,, \\ 1\,, & T > T_{1,CH}\,. \end{cases} \tag{4}$$

The representive degree of dehydration ξ_{dehyd} results from the two degrees ξ_{CSH} and ξ_{CH} and their initial volume portion f_{CSH} and f_{CH}.

$$\xi_{dehyd}(T) = f_{CH} \cdot \xi_{CH}(T) + f_{CSH} \cdot \xi_{CSH}(T) \tag{5}$$

The temperature dependent evolution ξ_{dehyd} is shown in Fig. 3 and shows at the steep gradient at a temperature of about 780 K the immediate dehydration of portlandit.

3.3 Modelling the mechanical behaviour

The mechanical behavior of concrete at high temperatures is mainly influenced by three phenomena, the high pore pressure, the large thermal strain and the dehydration in the cement paste, which all are considered in the mechanical model. For the description of the deformation a linear kinematic relation between deformation gradient components and the strain tensor is assumed

$$\epsilon_{ij} = \tfrac{1}{2}\left(u_{i,j} + u_{j,i}\right) \tag{6}$$

This assumption can be used in the model, since only relatively small deformations occur in concrete at high temperatures.

The pore pressure is part of the momentum balance equation

$$0 = \nabla \cdot (\boldsymbol{\sigma} + \boldsymbol{I}\,(1 - S_w)\,b\,p_g) + \rho\,\boldsymbol{g} \tag{7}$$

by means of the Biot coefficient *b*, which describes the portion of pore pressure acting on the solid skeleton. The Biot coefficient depends on the temperature like the other model parameters and can be computed by an analytical multi-scale approach, see Ostermann (2012), Pichler *et al*. (2003).

The evolution of thermal strains follows a multi-scale formulation as function of temperature, see Ostermann (2012). The value of thermal strain is mainly governed by the extension of the concrete aggregates due to their large volumetric content and by the shrinkage of cement minerals as a consequence of dehydration, see Fig. 4.

The dehydration mainly influences the stress-strain-behaviour of concrete. The elastic properties are reduced during dehydration, since the cement paste between the aggregates is gradually dissolved. Furthermore, the limit stresses decreases similarly during dehydration, which is related to the tensile strength of concrete as well as the compressive strength. In the mechanical model for ambient temperatures, a composed crack surface enables a separate description of the tensile and compressive behaviour also with respect to the different damage evolution of these two types of loading, see Ostermann (2012). The isotropic damage gradually reduces the limit surface, see Fig. 5.

Fig. 5 shows the initial limit surfaces for the concrete and the damaged limit surface, as it evolves during the exposure to high temperatures.

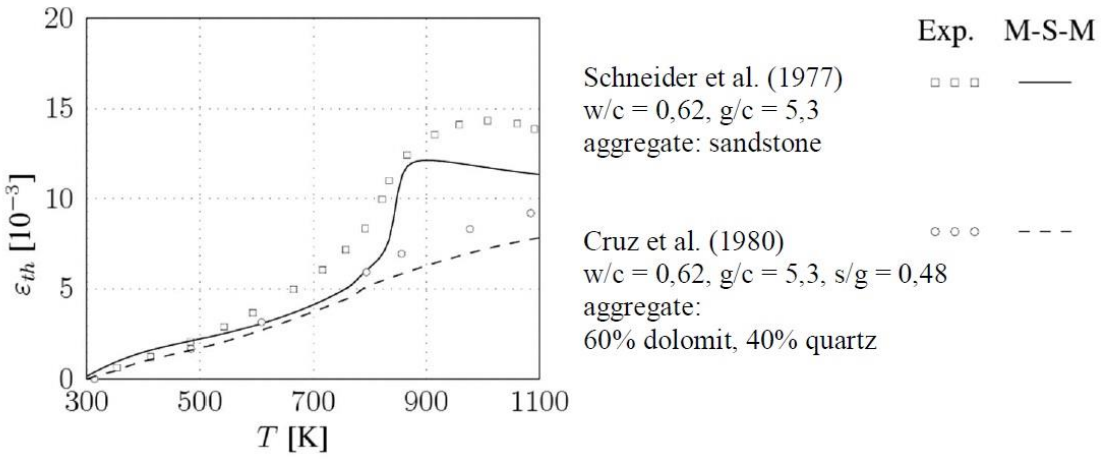

Fig. 4 Thermal strain

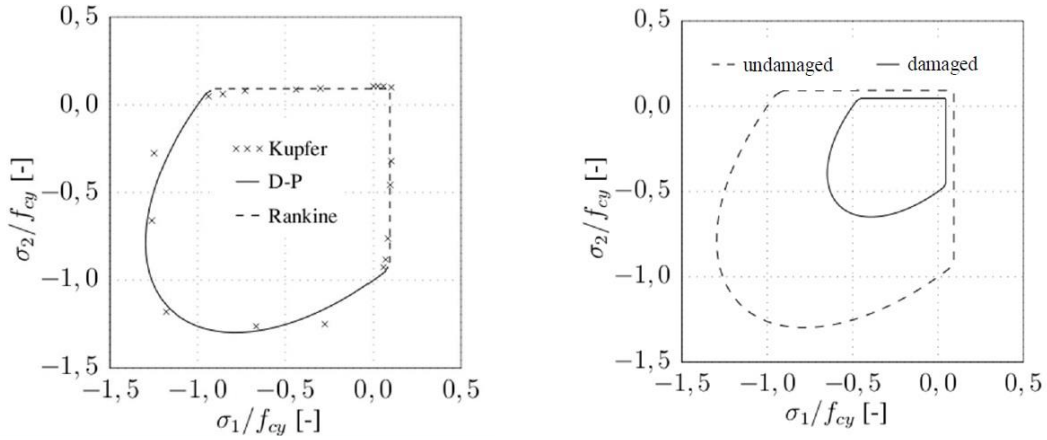

Fig. 5 Limit stress surface

Fig. 6 illustrates the evolution of local compressive normal stress σ_c with increasing strain. Left figure shows the irreversible part of strain ε_{ir} after relief of load. The influence of the chemical damage M_{chem} on the local stress-strain strain beviour is shown in the right figure.

The total damage consists of several damage components, which are deduced from the phenomena of mechanical behaviour in concrete at high temperatures. They can be distinguished between chemical damage M_{chem} due to thermal dehydration of cement paste, mechanical damage $M_{tensile}$ due to tension and mechanical damage M_{comp} due to compression. In this paper a multiplicative ansatz is used (Gawin *et al*. 2003).

$$M_{total} = M_{chem} \cdot M_{tensile} \cdot M_{comp}$$

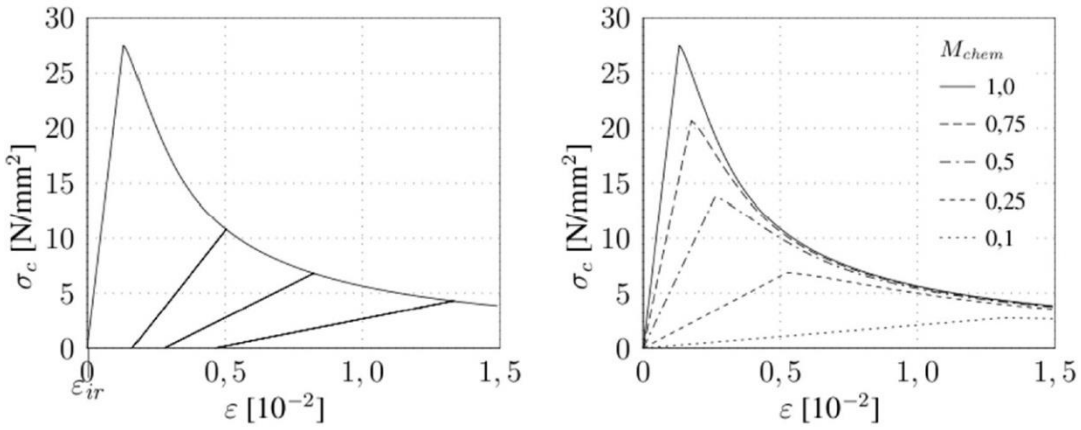

Fig. 6 Local stress-strain strain beviour

4. Numerical solution

The system of non-linear differential equations is written in terms of temperature, relative humidity, displacements, and the non-local variables. By defining a reference vapour pressure above the critical point of water, the relative humidity can be used as an independent variable for the whole temperature range. The discretisation of the coupled system of balance equations in space is realised by the Finite-Element-Method with quadrilateral elements with linear ansatz functions. The time derivative is discretised by the implicit Euler scheme.

4.1 Weak formulation of the governing equations

The set of balance equations is formulated in a weak form, in order to achieve the following global coupled system of equations

$$\mathbf{H}(z^{t_{n+1}}) \cdot \frac{\mathbf{z}^{t_{n+1}} - \mathbf{z}^{t_n}}{\Delta t} + \mathbf{K}(\mathbf{z}^{t_{n+1}}) \cdot \mathbf{z}^{t_{n+1}} = \mathbf{f}(\mathbf{z}^{t_{n+1}}) \tag{8}$$

with the global vector of nodal variables of the current time step $\mathbf{z}^{t_{n+1}}$ and the previous time step $\mathbf{z}^{t_n}$, which is linearised to solve it for the current time step with the Newton-Raphson method. The global matrices **H**, **K** and the global vector **f** consist of element matrices and vectors

$$\mathbf{H} = \sum_{i=1}^{N_{ele}} \mathbf{H}_{ele}\,,\ \mathbf{K} = \sum_{i=1}^{N_{ele}} \mathbf{K}_{ele}\,,\mathbf{f} = \sum_{i=1}^{N_{ele}} \mathbf{f}_{ele} \tag{9}$$

The element matrices are composed of element matrices representing the balance equations.

$$\mathbf{K}_{ele} = \begin{bmatrix} \mathbf{K}_{ele,p_a\,p_a} & \mathbf{K}_{ele,p_a\,\varphi} & \mathbf{K}_{ele,p_a\,T} & 0 & 0 & 0 \\ \mathbf{K}_{ele,\varphi\,p_a} & \mathbf{K}_{ele,\varphi\,\varphi} & \mathbf{K}_{ele,\varphi\,T} & 0 & 0 & 0 \\ \mathbf{K}_{ele,T\,p_a} & \mathbf{K}_{ele,T\,\varphi} & \mathbf{K}_{ele,T\,T} & 0 & 0 & 0 \\ \mathbf{K}_{ele,\mathbf{u}\,p_a} & \mathbf{K}_{ele,\mathbf{u}\,\varphi} & \mathbf{K}_{ele,\mathbf{u}\,T} & \mathbf{K}_{ele,\mathbf{u}\,\mathbf{u}} & 0 & 0 \\ 0 & 0 & 0 & 0 & \mathbf{K}_{ele,\bar{\boldsymbol{\varepsilon}}_{ir,R}\,\bar{\boldsymbol{\varepsilon}}_{ir,R}} & 0 \\ 0 & 0 & 0 & 0 & 0 & \mathbf{K}_{ele,\bar{\lambda}_{DP}\,\bar{\lambda}_{DP}} \end{bmatrix},$$

$$\mathbf{H}_{ele} = \begin{bmatrix} \mathbf{H}_{ele,p_a\,p_a} & \mathbf{H}_{ele,p_a\,\varphi} & \mathbf{H}_{ele,p_a\,T} & \mathbf{H}_{ele,p_a\,\mathbf{u}} & 0 & 0 \\ \mathbf{H}_{ele,\varphi\,p_a} & \mathbf{H}_{ele,\varphi\,\varphi} & \mathbf{H}_{ele,\varphi\,T} & \mathbf{H}_{ele,\varphi\,\mathbf{u}} & 0 & 0 \\ \mathbf{H}_{ele,T\,p_a} & \mathbf{H}_{ele,T\,\varphi} & \mathbf{H}_{ele,T\,T} & \mathbf{H}_{ele,T\,\mathbf{u}} & 0 & 0 \\ \mathbf{H}_{ele,\mathbf{u}\,p_a} & \mathbf{H}_{ele,\mathbf{u}\,\varphi} & \mathbf{H}_{ele,\mathbf{u}\,T} & \mathbf{H}_{ele,\mathbf{u}\,\mathbf{u}} & 0 & 0 \\ 0 & 0 & 0 & 0 & 0 & 0 \\ 0 & 0 & 0 & 0 & 0 & 0 \end{bmatrix},$$

$$\mathbf{z}_{ele} = \left[\mathbf{z}_{ele,p_a}\,,\ \mathbf{z}_{ele,\varphi}\,,\ \mathbf{z}_{ele,T}\,,\ \mathbf{z}_{ele,\mathbf{u}}\,,\ \mathbf{z}_{ele,\bar{\boldsymbol{\varepsilon}}_{ir,R}}\,,\ \mathbf{z}_{ele,\bar{\lambda}_{DP}}\right]^T,$$

$$\mathbf{g}_{ele} = \left[\mathbf{f}_{ele,p_a}\,,\ \mathbf{f}_{ele,\varphi}\,,\ \mathbf{f}_{ele,T}\,,\ \mathbf{f}_{ele,\mathbf{u}}\,,\ \mathbf{f}_{ele,\bar{\boldsymbol{\varepsilon}}_{ir,R}}\,,\ \mathbf{f}_{ele,\bar{\lambda}_{DP}}\right]^T.$$

The element matrices for the transport of dry air read as

$$\mathbf{H}_{ele,\,p_a\,p_a} = \int_{\Omega_{ele}} \mathbf{N}_{p_a}^{\mathrm{T}}\, n\,(1-S_w)\,\frac{\partial \rho_a}{\partial p_a}\,\mathbf{N}_{p_a}\,\mathrm{d}\mathbf{x}\,,$$

$$\mathbf{H}_{ele,\,p_a\,\varphi} = \int_{\Omega_{ele}} \mathbf{N}_{p_a}^{\mathrm{T}}\,(-n\,\rho_a)\,\frac{\partial S_w}{\partial \varphi}\,\mathbf{N}_{\varphi}\,\mathrm{d}\mathbf{x}\,,$$

$$\begin{aligned}\mathbf{H}_{ele,\,p_a\,T} = \int_{\Omega_{ele}} \mathbf{N}_{p_a}^{\mathrm{T}} \Bigg(& -n\,\rho_a\,\frac{\partial S_w}{\partial T} + n\,(1-S_w)\,\frac{\partial \rho_a}{\partial T} + (1-S_w)\,\rho_a \frac{\partial n}{\partial \xi_{deh}}\frac{\partial \xi_{deh}}{\partial T} \\ & -(1-s_w)\rho_a \frac{1-n}{\rho_{s,beton}}\left(\frac{\partial c_{v,deh}}{\partial \xi_{deh}}\frac{\partial \xi_{deh}}{\partial T} - \frac{\partial \rho_{s,beton}}{\partial \xi_{deh}}\frac{\partial \xi_{deh}}{\partial T} - \frac{\partial \rho_{s,beton}}{\partial T}\right)\Bigg)\,\mathbf{N}_T\,\mathrm{d}\mathbf{x}\,,\end{aligned}$$

$$\mathbf{H}_{ele,\,p_a\,\mathbf{u}} = \int_{\Omega_{ele}} \mathbf{N}_{p_a}^{\mathrm{T}}\,(1-S_w)\,\rho_a\,\nabla\cdot\mathbf{N}_{\mathbf{u}}\,\mathrm{d}\mathbf{x}\,,$$

$$\mathbf{K}_{ele,\,p_a\,p_a} = \int_{\Omega_{ele}} \nabla\mathbf{N}_{p_a}^{\mathrm{T}} \left(\rho_a\,\frac{\mathbf{k}\,k_{rg}}{\mu_g} + \rho_a\,\mathbf{D}_{diff}\,\frac{p_v}{(p_a+p_v)^2}\right)\nabla\mathbf{N}_{p_a}\,\mathrm{d}\mathbf{x}\,,$$

$$\mathbf{K}_{ele,\,p_a\,\varphi} = \int_{\Omega_{ele}} \nabla\mathbf{N}_{p_a}^{\mathrm{T}} \left(\rho_a\,\frac{\mathbf{k}\,k_{rg}}{\mu_g}\,\frac{\partial p_v}{\partial \varphi} - \rho_a\,\mathbf{D}_{diff}\,\frac{p_a}{p_a+p_v}\,\frac{\partial p_v}{\partial \varphi}\right)\nabla\mathbf{N}_{p_a}\,\mathrm{d}\mathbf{x}\,,$$

$$\mathbf{K}_{ele,\,p_a\,T} = \int_{\Omega_{ele}} \nabla\mathbf{N}_{p_a}^{\mathrm{T}} \left(\rho_a\,\frac{\mathbf{k}\,k_{rg}}{\mu_g}\,\frac{\partial p_v}{\partial T} - \rho_a\,\mathbf{d}_v\,\frac{p_a}{(p_a+p_v)}\,\frac{\partial p_v}{\partial T}\right)\nabla\mathbf{N}_{p_a}\,\mathrm{d}\mathbf{x}$$

The element matrices for the transport of water and vapour are

$$\mathbf{H}_{ele,\,\varphi\,\varphi} = \int_{\Omega_{ele}} \mathbf{N}_{\varphi}^{\mathrm{T}} \left(n\,(\rho_w - \rho_v)\,\frac{\partial S_w}{\partial \varphi} + n\,(1-S_w)\,\frac{\partial \rho_v}{\partial \varphi} \right) \mathbf{N}_{\varphi}\,\mathrm{dx}\,,$$

$$\begin{aligned}\mathbf{H}_{ele,\,\varphi\,T} = \int_{\Omega_{ele}} \mathbf{N}_{\varphi}^{\mathrm{T}} \Bigg(& n\,(\rho_w - \rho_v)\,\frac{\partial S_w}{\partial T} + n\,(1-S_w)\,\frac{\partial \rho_v}{\partial T} + n\,S_w \frac{\partial \rho_w}{\partial T} \\ & - (S_w\,\rho_w + (1-S_w)\,\rho_v)\,\frac{1-n}{\rho_{s,beton}} \left(\left(\frac{\partial c_{v,deh}}{\partial \xi_{deh}} - \frac{\partial \rho_{s,beton}}{\partial \xi_{deh}} \right) \frac{\partial \xi_{deh}}{\partial T} - \frac{\partial \rho_{s,beton}}{\partial T} \right) \\ & + (S_w\,\rho_w + (1-S_w)\,\rho_v)\,\frac{\partial n}{\partial \xi_{deh}} \frac{\partial \xi_{deh}}{\partial T} - \frac{\partial c_{v,deh}}{\partial \xi_{deh}} \frac{\partial \xi_{deh}}{\partial T} \Bigg)\, \mathbf{N}_T\,\mathrm{dx}\,,\end{aligned}$$

$$\mathbf{H}_{ele,\,\varphi\,\mathbf{u}} = \int_{\Omega_{ele}} \mathbf{N}_{\varphi}^{\mathrm{T}}\,(S_w\,\rho_w + (1-S_w)\,\rho_v)\,\nabla \cdot \mathbf{N}_{\mathbf{u}}\,\mathrm{dx}\,,$$

$$\mathbf{K}_{ele,\,\varphi\,p_a} = \int_{\Omega_{ele}} \nabla \mathbf{N}_{\varphi}^{\mathrm{T}} \left(\rho_w \frac{\mathbf{k}_w}{\mu_w} + \rho_v \frac{\mathbf{k}_g}{\mu_g} + \rho_v\,\mathbf{D}_{diff}\,\frac{p_v}{(p_a+p_v)^2} \right) \nabla \mathbf{N}_{p_a}\,\mathrm{dx}\,,$$

$$\begin{aligned}\mathbf{K}_{ele,\,\varphi\,\varphi} = \int_{\Omega_{ele}} \nabla \mathbf{N}_{\varphi}^{\mathrm{T}} & \left(\rho_w \frac{\mathbf{k} k_{rw}}{\mu_w} \left(\frac{\partial p_v}{\partial \varphi} - \frac{\partial p_c}{\partial \varphi} \right) + \rho_v \frac{\mathbf{k} k_{rg}}{\mu_g} \frac{\partial p_v}{\partial \varphi} + \rho_v\,\mathbf{D}_{diff}\,\frac{p_a}{p_a+p_v}\,\frac{\partial p_v}{\partial \varphi} \right) \\ & \nabla \mathbf{N}_{\varphi}\,\mathrm{dx}\,,\end{aligned}$$

$$\begin{aligned}\mathbf{K}_{ele,\,\varphi\,T} = \int_{\Omega_{ele}} \nabla \mathbf{N}_{\varphi}^{\mathrm{T}} & \left(\rho_w \frac{\mathbf{k} k_{rw}}{\mu_w} \left(\frac{\partial p_v}{\partial T} - \frac{\partial p_c}{\partial T} \right) + \rho_v \frac{\mathbf{k} k_{rg}}{\mu_g} \frac{\partial p_v}{\partial T} + \rho_v\,\mathbf{D}_{diff}\,\frac{p_a}{p_a+p_v}\,\frac{\partial p_v}{\partial T} \right) \\ & \nabla \mathbf{N}_T\,\mathrm{dx}\end{aligned}$$

The element matrices for the transport of energy read as

$$\mathbf{H}_{ele,\,T\,\varphi} = \int_{\Omega_{ele}} \mathbf{N}_T^{\mathrm{T}}\,n\,\rho_w\,\frac{\partial S_w}{\partial \varphi}\,\Delta h_{vap}\,\mathbf{N}_{\varphi}\,\mathrm{dx}$$

$$\begin{aligned}\mathbf{H}_{ele,\,T\,T} = \int_{\Omega_{ele}} \mathbf{N}_T^{\mathrm{T}} & \left(\frac{\partial \Delta H_{dehdr}}{\partial \xi_{deh}} \frac{\partial \xi_{deh}}{\partial T} + \left(n\,\rho_w \frac{\partial S_w}{\partial T} + n\,S_w \frac{\partial \rho_w}{\partial T} \right) \Delta h_{vap} \right. \\ & + \left(-S_w\,\rho_w \frac{1-n}{\rho_{s,beton}} \left(\left(\frac{\partial c_{v,deh}}{\partial \xi_{deh}} - \frac{\partial \rho_{s,beton}}{\partial \xi_{deh}} \right) \frac{\partial \xi_{deh}}{\partial T} - \frac{\partial \rho_{s,beton}}{\partial T} \right) \right) \Delta h_{vap} \\ & \left. + \left(S_w\,\rho_w \frac{\partial n}{\partial \xi_{deh}} \frac{\partial \xi_{deh}}{\partial T} - \frac{\partial c_{v,deh}}{\partial \xi_{deh}} \frac{\partial \xi_{deh}}{\partial T} \right) \Delta h_{vap} \right) \mathbf{N}_T\,\mathrm{dx}\,,\end{aligned}$$

$$\mathbf{H}_{ele,\,T\,\mathbf{u}} = \int_{\Omega_{ele}} \mathbf{N}_T^{\mathrm{T}}\,S_w\,\rho_w\,\Delta h_{vap}\,\nabla \cdot \mathbf{N}_{\mathbf{u}}\,\mathrm{dx}\,,$$

$$\mathbf{K}_{ele,\,T\,p_a} = \int_{\Omega_{ele}} \nabla \mathbf{N}_T^{\mathrm{T}}\,\rho_w \frac{\mathbf{k} k_{rw}}{\mu_w}\,\Delta h_{vap}\,\nabla \mathbf{N}_{p_a}\,\mathrm{dx}\,,$$

$$\mathbf{K}_{ele,\,T\,\varphi} = \int_{\Omega_{ele}} \nabla \mathbf{N}_T^{\mathrm{T}} \left(\rho_w \frac{\mathbf{k} k_{rw}}{\mu_w} \left(\frac{\partial p_v}{\partial \varphi} - \frac{\partial p_c}{\partial \varphi} \right) \right) \Delta h_{vap}\,\nabla \mathbf{N}_{\varphi}\,\mathrm{dx}\,,$$

$$\begin{aligned}\mathbf{K}_{ele,\,T\,T} = & \int_{\Omega_{ele}} \nabla \mathbf{N}_T^{\mathrm{T}} \left(\lambda_{beton} + \rho_w \frac{\mathbf{k} k_{rw}}{\mu_w} \left(\frac{\partial p_v}{\partial T} - \frac{\partial p_c}{\partial T} \right) \right) \Delta h_{vap}\,\nabla \mathbf{N}_T\,\mathrm{dx} \\ & + \int_{\Omega_{ele}} \mathbf{N}_T^{\mathrm{T}}\,(C_{pg}\,\mathbf{v}_g + C_{pw}\,\mathbf{v}_w) \cdot \nabla \mathbf{N}_T\,\mathrm{dx}\,.\end{aligned}$$

$$\mathbf{f}_{ele,\,T} = \int_{\Gamma_{ele}^{T_\infty}} \mathbf{N}_T^{\mathrm{T}} \left(e\,\sigma_0 \left(T^4 - {T_\infty}^4 \right) + a_T \left(T - T_\infty \right) \right) \mathrm{d}\mathbf{x} \; .$$

4.2 Solution strategy for the coupled system

Due to the coupling property of the system of the balance equations a monolithic approach for the solution as shown in Fig. 7 is preferred to the staggered method, see Gawin *et al*. (2003).The system of coupled equations is solved iteratively by applying a Newton-Raphson algorithm.

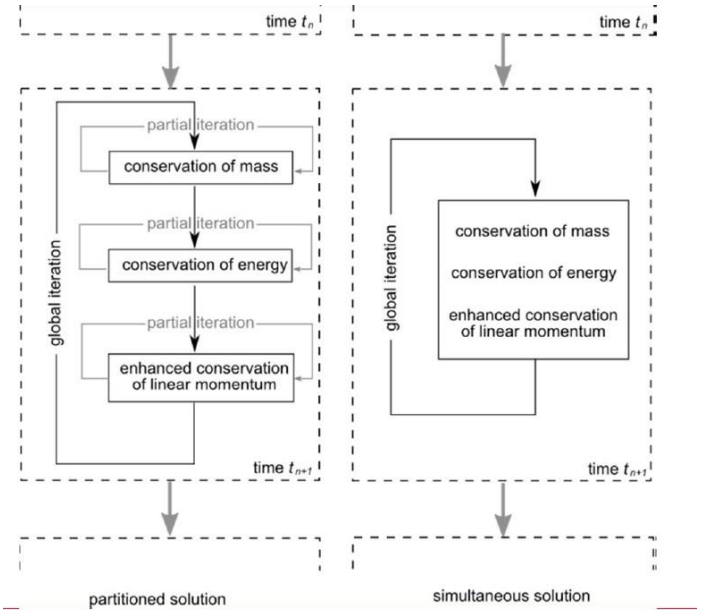

Fig. 7 Solution strategies for the coupled system

5. Numerical analysis of concrete structures

The presented model allows a macroscopic, numerical simulation of the transport processes and the behaviour of concrete structures subject to high temperatures. For the numerical analysis, the influence of material properties on the high-temperature behaviour is examined as a first step. From these results, selected concrete structures are numerically analysed.

5.1 Influence of material properties

Due to the complexity of the model, it is difficult to predict a priori the influence of single parameters on the complete system. One of the most important parameters is the permeability, since it mainly governs the vapour transport in the pores. Fig. 8 demonstrates the influence of

permeability on the pore pressure. Because of spalling at large pore pressures, the increase of the maximum pressure flattens $p_{v,max}$ for very small values of permeabilityk_0. The other parameters show less influence on the high temperature behaviour of concrete, see Ostermann (2003). Furthermore, Fig. 8 shows the maximum pore pressure for different values of permeability k_0 for the case, that the maximum tensile stress f_t is not limited.

5.2 Analysis of concrete columns

In this section, the results of the numerical simulation for different geometries of concrete columns subject to high temperatures are shown. The results illustrate that the type of geometry influences significantly the high-temperature behaviour.

Here, a quadratic cross-section, see Fig. 10, is analysed with an ISO-temperature-time-curve for the evolution of temperature

$$T_\infty(t) = 293{,}15 + 345 \cdot \ln(8 \cdot t + 1)$$

with t in [min]. The boundary and initial conditions are given in Fig. 9.

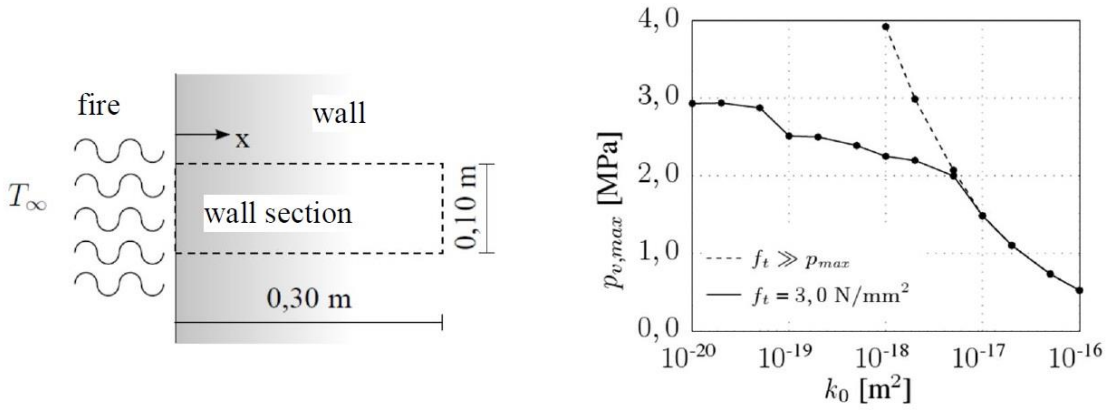

Fig. 8 Influence of permeability on pressure peak value

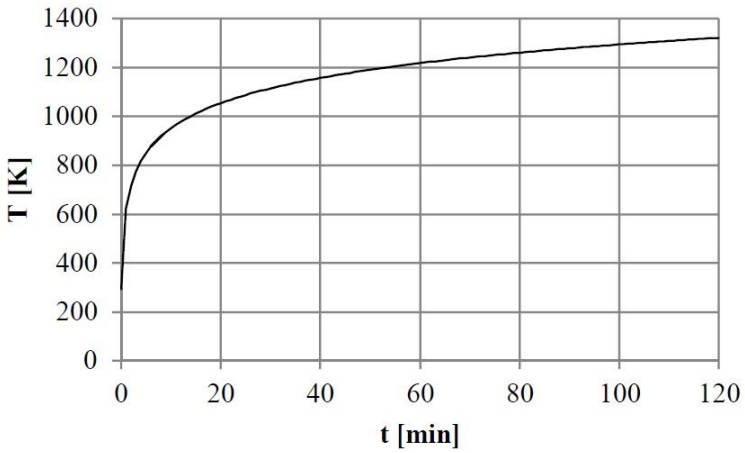

Fig. 9 ISO-fire-curve

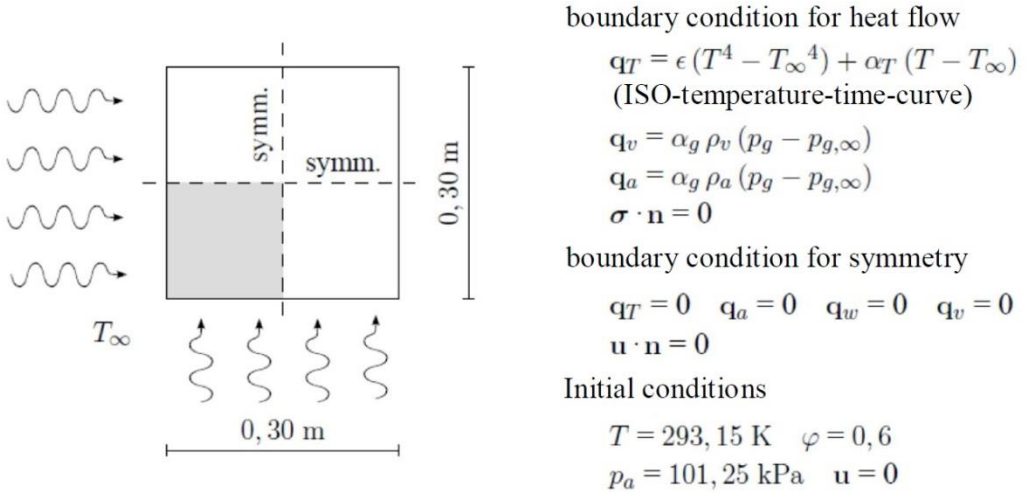

Fig. 10 Cross-section with boundary and initial conditions

For the numerical analysis of the cross-section a concrete C25 is used. Hence, the model parameter for the macroscopic model are chosen as follows

$E_{beton} = 37500\ \mathrm{N/mm^2}$ $\quad k_0 = 10^{-16}\mathrm{m^2}$
$\nu = 0{,}2$ $\quad \lambda_0 = 1{,}0\ \mathrm{W/(m\,K)}$
$f_t = 2{,}75\ \mathrm{N/mm^2}$ $\quad w/z = 0{,}5$
$f_c = 37{,}5\ \mathrm{N/mm^2}$

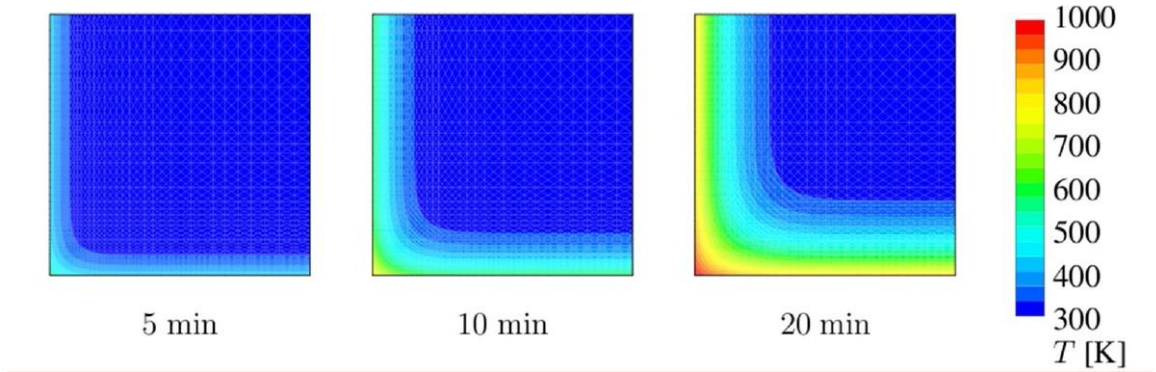

Fig. 11 Evolution of temperature at different time stages

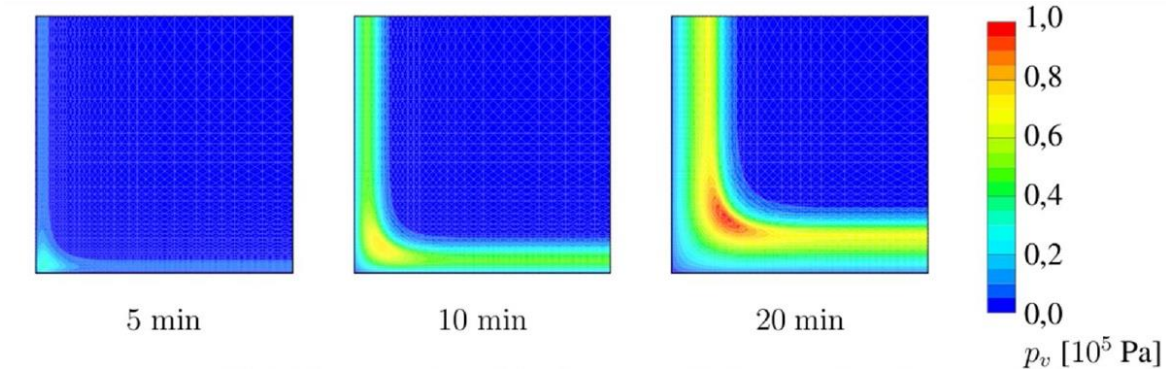

Fig. 12 Evolution of vapour pressure at different time stages

Fig. 11 shows the temperature distribution at various points in time which covers the average duration of a fire accident. The temperature at the edge increases more faster than other boundary regions, since external heat acts on the two sides of the edge. The vapour pressure increases locally to a pressure clog close to the boundary as a consequence of the rapid temperature rise. Due to the higher temperature values at the edge, here, the vapour pressure reaches its maximum values, see Fig. 12.

The evolution of the temperature leads to high stresses within the structure. First, the high temperature at the boundary effects large thermal strains and large strain gradients, which affect the structural behaviour. Additionally, the high pore pressure resulting from released vapour increases the stress in the structure. The large stresses lead to mechanical damage, since the limitation of stresses is coupled with the evolution of damage. Furthermore chemical damage from the dehydration of cement minerals contributes to the increase of the total damage close to the heated boundary. The damage distribution in Fig.13 shows the damage growth at the heated boundary, which mainly originates from dehydration, and the damage zone in the interior due to internal stresses from vapour pressure and thermal strain.

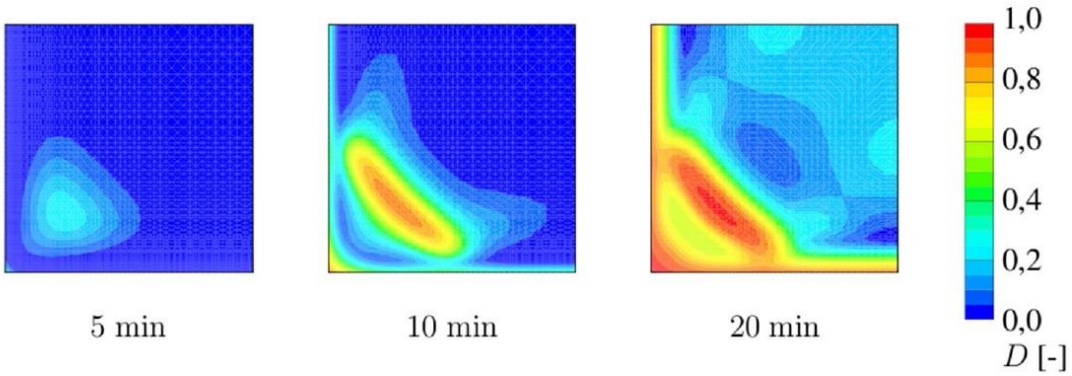

Fig. 13 Evolution of total damage at different time stages

6. Conclusions

The theoretical foundations of the presented model are the balance equations, which are derived with the theory of porous media. For the present model, the conservation equations of mass of dry air, vapour, pore water, of linear momentum, and of energy are required to describe the transport processes and the mechanical behaviour. Due to the interaction of the transport processes, the chemical reactions and the mechanical behavior the resulting non-linear system of equations is strongly coupled, which requires an iterative solution strategy. The results show the influence of the local material properties as the tensile strength and the influence of the global geometry on the structural behaviour at high temperatures.

Acknowledgments

Financial support was provided by the German National Science Foundation (DFG) grant no. Di-389-16-2 and by the German Academic Exchange Service (DAAD) grant no. D/05/47060. These supports are gratefully acknowledged.

References

Bažant, Z., Chern, J.C. and Thonguthai, W. (1981), "Finite element program for moisture and heat transfer in heated concrete", *Nucl. Eng. Des*., **68**(1), 61-70.

Cerny, R., Totova, M., Podebradska, J., Torman, J., Drchalova, J. and Rovnanikova, P. (2003), "Thermal and hygric properties of Portland cement mortar after high temperature exposure combined with compressive stress", *Cement. Concrete Res*., **33**(9), 1347-1355.

Cruz, C.R. and Gillen, M. (1980), "Thermal Expansion of Portland Cement Paste, Mortar and Concrete at High Temperatures". *Fire Mater.*, **4**, 66-70.

Gawin, D., Majorana, C. and Schrefler, B. (1999), "Numerical analysis of hygro-thermal behaviour and damage of concrete at high temperature", *Mech. Cohes.-Frict.Mater*., **4**, 37-74.

Gawin, D., Pesavento, F. and Schrefler, B.A. (2003), "Modelling of hygro-thermal behavior of concrete at high temperature with thermo-chemical and mechanical material degradation", *Comput. Method. Appl. M.*, **192**(13-14), 1731-1771.

International Association for the Properties of Water and Steam (1994), IAPWS Release on Surface Tension of Ordinary Water Substance.

Khoury, G.A. (2006), "Strain of heated concrete during two thermal cycles. Part 3: isolation of strain components and strain model development", *Mag. Concrete. Res*., **58**(7), 421-435.

Lewis, R. and Schrefler, B. (1998), *The finite element method in the static and dynamic deformation and consolidation of porous Media*, Wiley.

Monlouis-Bonnaire, J., Verdier, J. and Perrin, B. (2004), "Prediction of the relative permeability to gas flow of cement-based materials", *Mag. Concrete. Res*., **34**(5), 737-744.

Ostermann, L. (2012), *Hochtemperaturverhalten von Beton - Gekoppelte Mehrfeld-Modellierung und numerische Analyse*, Institut für Statik, TU Braunschweig

Peerlings, R.H.J., de Borst, R., Brekelmans, W.A.M. and Geers, M.G.D. (1998), "Gradient-enhanced damage modelling of concrete fracture", *Mech. Cohes.-Frict. Mater*., **3**(4), 323-342.

Pichler, C., Lackner, R. and Mang, H.A. (2007), "A multiscale micromechanics model for the auto genous-shrinkage deformation of early-age cement-based materials", *Eng. Fract. Mech*., **74**, 34-58.

Schneider, U. and Weiß, R. (1977),“Kinetische Betrachtungen über den thermischen Abbau zementgebundener Betone und dessen mechanische Auswirkungen”, *Cement. Concrete Res*., **7**(3), 259-268.